

Predicting the Synthesizability of Double Perovskite Halides via Interface Reaction Pathfinding

Woongchan Kim, Hyeon Woo Kim, Han Uk Lee, Min Sung Kang, Dong Won Jeon, Soo Won Heo, and Sung Beom Cho*



Cite This: *Chem. Mater.* 2024, 36, 5904–5911



Read Online

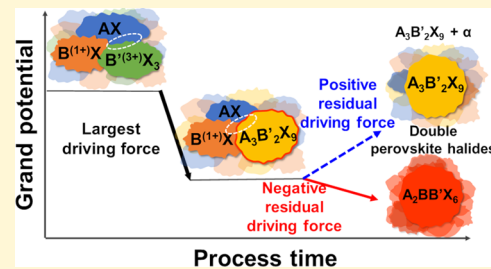
ACCESS |

Metrics & More

Article Recommendations

Supporting Information

ABSTRACT: Recent advancements in high-throughput screening and data mining have significantly expedited the discovery of new multicomponent materials, replacing the traditionally time-consuming trial-and-error methodologies. However, accurately predicting their synthesizability remains a formidable challenge, primarily due to discrepancies between theoretical predictions and experimental processes. Theoretical predictions are focused on the stability of the final crystal structure, like energy above hull and structural factors. Experimental evolution process has complex conditions: temperature, pressure, and reaction mechanics like interface reaction. This study demonstrates that incorporating reaction pathways markedly enhances the synthesizability prediction accuracy for double perovskite halides. We predict intermediates and synthetic pathways through a detailed analysis of interface reaction mechanisms and chemical reaction networks. Specifically, the formation of the $A_3B'_2X_9$ intermediate is predicted with a high driving force during the precursor's interface reaction. Subsequently, the residual Gibbs free energy of formation necessary for the transition from the $A_3B'_2X_9$ intermediate to double perovskite halides is shown to be crucial in determining the synthesizability. This approach surpassed existing structural factor-based approaches in accuracy, enabling us to predict synthesizable double perovskite halides such as Cs_2AgYCl_6 and Cs_2KInCl_6 more effectively. These findings show the critical role of incorporating reaction mechanisms into synthesizability predictions, thereby facilitating the discovery of new multicomponent materials.



1. INTRODUCTION

In recent years, the advancement of rational material design techniques, including high-throughput screening and data mining, has significantly accelerated the discovery of new materials, replacing the traditionally time-consuming trial-and-error methodologies.^{1,2} Noteworthy examples include diverse application fields such as luminescent materials, solid-state electrolyte materials, and so on.^{3–6} The materials were first predicted computationally to possess superior properties compared to existing ones and were subsequently synthesized experimentally. However, a major challenge in these *in silico* approaches is their low synthesis success rate; about 90% of materials remain unrealized in synthetic form.⁷ This issue is particularly pronounced in the prediction of double perovskite halides, where the chemical space is vast and highly tunable.⁸ The root of the problem lies in the gap between theoretical prediction methods and experimental synthesis. Theoretical methods depend on indirect metrics like energy above hull for thermodynamic stability and on structural factors where the tolerance factor measures resemblance to cubic perovskite and the octahedral factor predicts stable octahedra formation;^{9,10} however, those factors cannot fully represent complex real-world phase competition and evolution, such as the appearance of intermediate in nucleation and growth stage.^{11,12} Addressing this disconnect to enhance the predictive accuracy of materials'

synthesizability is critical for the success of this *in silico* approach.

Recent research has significantly enhanced our understanding of the mechanisms underlying intermediate phase formation during solid-state synthesis processes.¹³ This is achieved by the use of *in situ* X-ray diffraction methods, which allowed researchers to monitor the synthesis as it unfolds step-by-step. The synthesis process is characterized by a series of sequential intermediate reactions, governed by interface reaction energetics. For instance, in the Na–Co–O system, the initial reaction between the precursors Na_2O_2 and CoO forms $NaCoO_2$ as the dominant phase due to its strong thermodynamic driving force. This is followed by the evolution of the final $Na_xCo_yO_z$ product through further reactions of $NaCoO_2$ with residual precursors and oxygen gas in a chamber. Another example is the synthesis of $YBa_2Cu_3O_{6.5}$,¹⁴ a well-known superconductor from Y_2O_3 , BaO, and CuO precursors. These cases illustrate that intermediate phases tend to form at

Received: December 29, 2023

Revised: May 20, 2024

Accepted: May 20, 2024

Published: June 5, 2024



interfaces where the thermodynamic driving force is most substantial. However, the formation of the final phase is more influenced by kinetics, as the residual thermodynamic driving force is lower. Similarly, by pathfinding the synthesis process of a target material and understanding the involved thermodynamic driving forces, we can attain more accurate theoretical predictions of its synthesizability.

Double perovskite halides are a material group that has been intensively studied with theoretical predictions; however, experimental synthesis is sluggish compared to their rich prediction. This group of materials follows the $A_2B^{(1+)}B'^{(3+)}X_6$ formula, where A is positively charged and arranged in a cuboctahedral coordination. Both B and B', carrying positive charges, form octahedral structures with adjacent anions. The X component typically serves as an anion and is primarily found in groups 15(VA) and 16(VIA) of the periodic table. With a double perovskite structure, the A, B, and B' positions can be easily substituted, leading to the flexibility of design spaces with diverse properties. To identify promising candidates among these materials, numerous computational calculations have been performed to find high-performance and stable double perovskite halides.^{15–19} However, a challenge lies in the limited number of predicted double perovskite halides that have been experimentally reported. This issue stems from the predictions relying solely on the structural stability or the thermodynamic stability of the final phase, whereas there is significant room for improvement if the predictions incorporate an understanding of the synthesis process.

In this study, we performed density functional theory (DFT) calculations for intermediate reaction pathfinding, aiming to bridge the gap between theoretical and experimental synthesizability. Our focus was on the $A_2B^{(1+)}B'^{(3+)}X_6$ double perovskites, which is a material rich in theoretical predictions yet scarcely synthesized experimentally. We propose that the formation of the $A_3B'^{(3+)}X_9$ intermediate phase through the interface reaction mechanism is a crucial initial step in synthesizing double perovskite halides. We designed the entire reaction pathway using a chemical reaction network incorporating the Gibbs free energy of formation from the precursor to the final product. Our findings highlight that the residual Gibbs free energy of formation from the $A_3B'^{(3+)}X_9$ intermediates to the final phase is a key factor in determining the synthesizability, owing to its higher thermodynamic driving force compared to other intermediates. We validated this approach against previously reported methods, demonstrating its relatively high accuracy compared to predictions based solely on structural factors. These results underscore the importance of considering sequential intermediate reactions from a thermodynamic perspective, especially given the challenges in the experimental verification of these intermediate stages.

2. METHODS

The DFT calculations were performed with the Vienna Ab initio Simulation Package (VASP).²⁰ The projector-augmented wave (PAW) method was used to take electron–ion interactions into account.²¹ The generalized gradient approximation (GGA) within the Perdew–Burke–Ernzerhof (PBE) was used for the exchange–correlation potential.²² A cutoff energy of 520 eV was used. For structure optimization, Hellmann–Feynman forces were in the range of 0.01 eV/Å. After structure relaxation, r2SCAN was used to account for electron–ion interactions to perform more accurate electronic structure calculations.²³ This method ensures numerical stability and

facilitates computation of more precise formation energies. The Brillouin zone was sampled using a 100 k-points density per Å³ in the reciprocal lattice.

In the solid-state synthesis of double perovskite halides, it is important to take into account the temperature when calculating the formation energy, given that the investigated scenarios occur at temperatures higher than room temperature. To calculate the temperature-dependent formation energy, the Gibbs free energy was defined as

$$\Delta G_{\text{formation}}(T) = G_{\text{product}}(T) - G_{\text{reactant}}(T)$$

The entropy and enthalpy components that constitute the Gibbs free energy are temperature-dependent. However, a value that can be easily determined through a DFT calculation is the temperature-independent enthalpy (ground state). Consequently, if we separate the terms dependent on temperature from those that are not, we can express them as follows:

$$G(T) = G^\delta(T) + \Delta H_f (298 \text{ K})$$

To determine $G^\delta(T)$, we utilized the physical descriptor for the Gibbs energy of an inorganic crystalline solid through the SISSO method:^{24,25}

$$G^\delta(T) \left[\frac{\text{eV}}{\text{atom}} \right] = (-2.48 \times 10^{-4} \times \ln(V) - 8.94 \times 10^{-5} \text{ mV}^{-1}) \\ T + 0.181 \times \ln(T) - 0.882$$

where V is the calculated atomic volume (Å³/atom), m is the reduced atomic mass (amu), and T is the temperature (K). Based on this machine learning-based descriptor, the formation energy for each material was computed at 300 K within a closed system. In the Supporting Information, we validate the method's applicability to double perovskite halides using the Cs–Ag–Bi–Br system, achieving an average error of 0.015 eV/atom.

Utilizing the formation of intermediates during the final phase synthesis process, we track the reaction pathway and monitor the associated energy changes.¹³ To trace the reaction path, the reaction mechanism between precursors at an interface is applied. After distinguishing the intermediates, we employ the chemical reaction network (CRN) method to identify pathways leading to the formation of the final state of the reaction,²⁶ using the existing precursor and the corresponding intermediate phase as reactants. Among these pathways, we consider the feasible intermediates while excluding cases with formation energies of 0.05 eV/atom or lower. The study does not encompass an analysis of the activation energy. Given that the synthesis of these compounds typically occurs at temperatures below 400 °C, comparable to the thermal conditions observed in systems undergoing interface reactions—such as 400 °C in the Na–Co–O¹³ system and 500 °C in the Y–Ba–Cu–O¹⁴ system—it is suggested that the activation energy barrier is likely overcome under these conditions.

3. RESULTS

To understand the synthesis process and utilize it for predictive purposes, we analyzed the reported experimental attempts to synthesize double perovskite halides. Table 1 presents the double perovskite halides that have been experimentally attempted based on predictions. Focusing on Table 1, we found that the starting precursors are in the form of compounds AX, B⁽¹⁺⁾X, and B'⁽³⁺⁾X₃ in a 2:1:1 ratio and that they are mixed at high temperatures. Among the experimentally attempted cases, we found that the B-site within $A_2B^{(1+)}B'^{(3+)}X_6$ is critical to its synthesizability. In most of the successful cases, the B-site is either occupied by Ag⁺ or Na⁺. On the other hand, unsuccessful synthesis attempts include Cs₂CuInBr₆ and Cs₂CuInCl₆, and both of them have copper ions (Cu⁺) in the B-site. Therefore, from the previous

Table 1. Results and Precursors for Double Perovskite Halides That Attempted to Be Solid-State Synthesized^a

compound	experimental solid-state synthesis	precursors
Cs ₂ AgBiBr ₆	S ²⁷	CsBr, AgBr, BiBr ₃
Cs ₂ AgBiCl ₆	S ²⁷	CsCl, AgCl, BiCl ₃
Cs ₂ NaBiCl ₆	S ²⁸	CsCl, NaCl, BiCl ₃
Cs ₂ AgSbCl ₆	S ²⁹	CsCl, AgCl, SbCl ₃
Cs ₂ AgInCl ₆	S ³⁰	CsCl, AgCl, InCl ₃
Cs ₂ CuInBr ₆	U ³¹	CsBr, CuBr, InBr ₃
Cs ₂ CuInCl ₆	U ³¹	CsCl, CuCl, InCl ₃

^aPrecursors were attempted to be synthesized by consistently putting AX, B⁽¹⁺⁾X, and B'⁽³⁺⁾X₃ in stoichiometric ratios. Successful syntheses are labeled S, and unsuccessful syntheses are labeled U.

synthetic routes analysis,^{13,14} it is essential to analyze the role of B-site cations in the sequential reactions.

The solid-state synthesis of double perovskite halides typically starts with sequential interface reactions among the precursors, denoted in Table 1 as AX, B⁽¹⁺⁾X, and B'⁽³⁺⁾X₃. To understand the synthetic routes, it is essential to compare potential reactions among these three precursors. We therefore constructed every possible interface reaction between two precursors, taking into account stoichiometry and mass balance. For the intermediates of these reactions, we referenced data from the Materials Project, ICSD, and literature sources.^{2,32–34} In intermediate candidates, the first intermediate is determined by the reaction with the largest driving force. Subsequent intermediates or the final state continue to form until they achieve thermodynamic ground states driven by the residual driving force, as illustrated in Figure 1. This is an expected result from the experimental

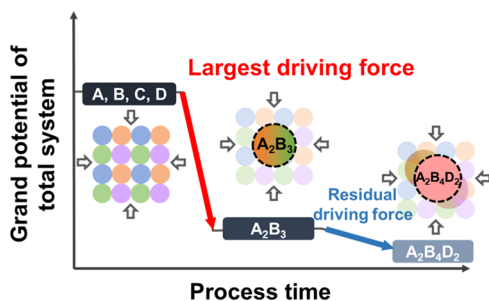


Figure 1. Schematic representation of a solid-state interface reaction demonstrating the stepwise formation process. Initially, the intermediate with the largest driving force forms at the precursors' interfaces, subsequently utilizing the residual driving force to transition into the final phase.

observation of the Na–Co–O and Y–Ba–Cu–O systems.^{13,14} In our study, the “A–B⁽¹⁺⁾–X system” refers to reactions between AX and B⁽¹⁺⁾X precursors, and the “A–B'⁽³⁺⁾–X system” refers to reactions between AX and B'⁽³⁺⁾X₃. The initial intermediate phase, determined by the reaction with the strongest driving force, could be from either the A–B⁽¹⁺⁾–X system or the A–B'⁽³⁺⁾–X system.

With the precursors and interface reaction energetics defined, we proceeded to calculate the Gibbs free energy of formation for the potential intermediates. The temperature-independent term was obtained through the DFT calculations, while the temperature-dependent term was determined using a machine learning-based descriptor.²⁵ We summarize the Gibbs free energies of formation for each calculated system in Figure

2. Notably, it is worth emphasizing that intermediates in the A–B'⁽³⁺⁾–X system exhibit a larger driving force when

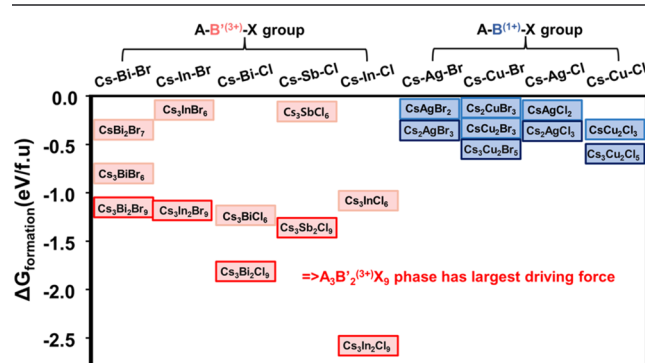


Figure 2. Gibbs free energy of formation of intermediates that can be generated by an interface reaction, calculated by DFT. Highlighted areas indicate intermediates with the largest driving force.

compared to their counterparts in the A–B⁽¹⁺⁾–X system. Thus, we anticipate that the A–B'⁽³⁺⁾–X system emerges as the more dominant initial intermediates as a first step. Furthermore, we found that a consistent trend of the intermediates with the largest driving force is likely to have an A₃B'₂⁽³⁺⁾X₉ phase consistently in the A–B'⁽³⁺⁾–X system. Due to the substantial driving forces associated with the A₃B'₂⁽³⁺⁾X₉ phase, we assume that the synthesis pathway for double perovskite halides should incorporate A₃B'₂⁽³⁺⁾X₉. This hypothesis is supported by the observation of the Cs₃In₂Br₉ and Cs₃In₂Cl₉ phase in X-ray diffraction (XRD) data from solid-state synthesis attempts of compounds such as Cs₂CuInBr₆ and Cs₂CuInCl₆.³¹

To understand the larger driving force of A₃B'₂⁽³⁺⁾X₉ in the A–B'⁽³⁺⁾–X system compared to that in the A–B⁽¹⁺⁾–X system, we conducted a thorough analysis of the structural change between precursors and intermediates. Our investigation revealed a considerable correlation between the driving force and the structural similarity of the B⁽¹⁺⁾ or B'⁽³⁺⁾ site framework in the intermediate product and the precursor (Figure 3). For the A–B'⁽³⁺⁾–X system, the spatial rearrangement of the polyhedral is notably less pronounced. Relative to the A–B⁽¹⁺⁾–X system, the displacement is reduced by approximately 0.51 Å, as detailed in the Supporting Information. And the polyhedra of B'⁽³⁺⁾X are already sparsely connected with 0D–2D connectivity. This is beneficial to form A₃B'₂⁽³⁺⁾X₉. When the additional halogen anion is included to meet the stoichiometry, the B'⁽³⁺⁾X polyhedron can easily capture the X anions and A cations by reshaping or tilting with minimal motion. For instance, BiCl₃ is characterized by a one-dimensional (1D) framework formed by [BiCl₅]²⁺ pentahedra, which exhibits relatively sparse coordination. When the intermediate Cs₃Bi₂Cl₉ forms from precursor BiCl₃, there is a transformation in the framework's dimensionality and an increment in coordination around the B'⁽³⁺⁾ site atom. The [BiCl₅]²⁺ polyhedral transforms into [BiCl₆]³⁺ octahedra with tilting, and relocates Cs⁺ cations in their interstitials. This is a relatively minor structural change. On the other hand, the polyhedral BX is more densely packed with three-dimensional (3D) connectivity and requires more bond-breaking of polyhedral or spatial rearrangement to include additional cations and anions. Regarding the Cs₂AgCl₃, the precursor AgCl forms a stable 3D configuration with a [AgCl₆]⁵⁺

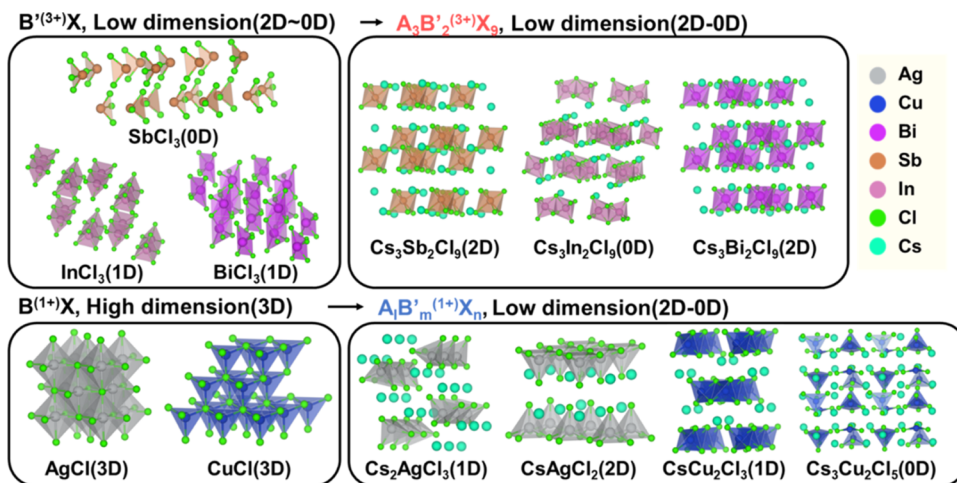


Figure 3. Crystal structures and dimensions of several precursors and intermediates. $B'(3+)X$ shows little dimensional change when reacting with AX , while $B'(1+)X$ changes from a stable 3D structure to a lower dimension.

octahedral framework, but the Cs_2AgCl_3 phase forms a $[AgCl_4]^{3+}$ tetrahedral 1D framework. Lots of polynomial bond-breaking is inevitable; thereby, it has relatively less driving force. Similar correlations were obtained from the $A-B'(3+)-X$ system and the $A-B(1+)-X$ system.

Based on the assumption that the intermediate $A_3B'_2(3+)X_9$ should be included in the synthesis path, we examined two of the most representative double perovskite cases, $Cs_2AgBiBr_6$ (synthesized) and $Cs_2CuInBr_6$ (not synthesized) (Figure 4). Utilizing the CRN, we defined possible reaction paths and then extracted paths containing the $A_3B'_2(3+)X_9$ phase. The CRN method is instrumental in predicting reaction pathways. It functions by using reactants and products as inputs to construct a network. In this network, potential phases are depicted as nodes, and the reactions between them are represented as edges. The CRN then identifies the most probable pathway for these inputs, considering the formation energy as a key weighting factor. For our study, we used AX , $B'(1+)X$, and $B'(3+)X_3$ as reactants, aiming to produce a compound with the formula $A_2B'(1+)B'(3+)X_6$. After generating various reaction pathways using this method, we specifically selected and listed those that included the $A_3B'_2(3+)X_9$ alignment with our theoretical framework.

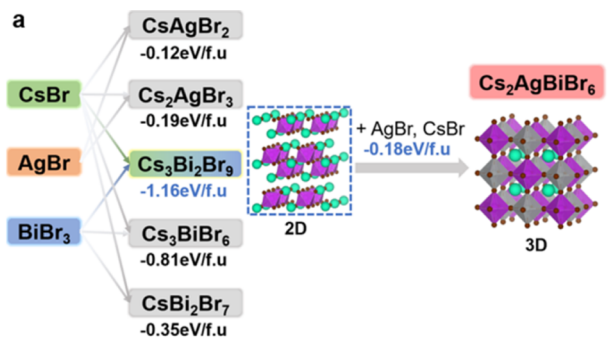
In the case of $Cs_2AgBiBr_6$, $Cs_3Bi_2Br_9$ forms with an energy of -1.16 eV per formula unit, followed by $Cs_2AgBiBr_6$, which requires a minimum energy of -0.18 eV per formula unit. Given the negative Gibbs free energies for both the pathway $Cs_3Bi_2Br_9 + CsBr + 2AgBr \rightarrow 2Cs_2AgBiBr_6$ and the pathways involving intermediates like Cs_2AgBr_3 , it is reasonable to predict the successful production of $Cs_2AgBiBr_6$. This path corresponds to the formation route characterized by minimal impurities.

On the other hand, the synthetic scenario for $Cs_2CuInBr_6$ presents a different picture. The Gibbs free energy needed to form intermediate $Cs_3In_2Br_9$ is spontaneous and relatively high at -1.15 eV per formula unit. However, the energy required to reach the final phase, $Cs_2CuInBr_6$, is even greater, at least 0.26 eV per formula unit. This positive energy requirement indicates that it does not occur spontaneously in forming the final phase. It aligns with experimental observations, wherein $Cs_3In_2Br_9$ and $CsCu_2Br_3$ were synthesized instead of the expected $Cs_2CuInBr_6$ as the final product.³¹ The high energy demand for transitioning from $Cs_3In_2Br_9$ to $Cs_2CuInBr_6$ is a

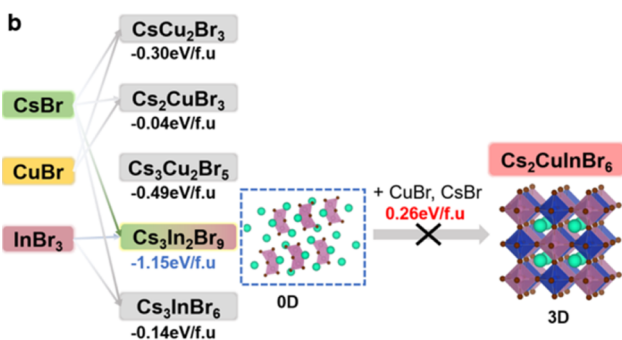
major contributing factor to this outcome. These insights imply the importance of considering the reaction path from phase $A_3B'_2(3+)X_9$ to final $A_2B'(1+)B'(3+)X_6$, along with the associated driving forces, as illustrated in Figure 5. This analysis not only clarifies the challenges in synthesizing certain double perovskites but also aids in predicting and strategizing more efficient synthesis pathways.

The $A_3B'_2(3+)X_9$ intermediate is generated at the interface between the AX and $B'(3+)X_3$ precursors, driven by a large driving force. Subsequently, the final state forms from the $A_3B'_2(3+)X_9$ intermediate, facilitated by the residual driving force. Through iterative reaction pathfinding for the candidates listed in Table 1, we have discerned that the residual Gibbs free energy of formation ($\Delta G_{\text{residual}}$) for the final $A_2B'(1+)B'(3+)X_6$ from the intermediate $A_3B'_2(3+)X_9$ is a critical determinant of synthesizability. This is evidenced by the correlation shown in Figure 6, where the $\Delta G_{\text{residual}}$ value is negative in cases of reported synthesis success and positive in cases where synthesis has failed. In successful cases, like $Cs_2AgBiBr_6$, $\Delta G_{\text{residual}}$ consistently shows a negative value across various pathways, indicating an energetically favorable process. This trend holds true even when an intermediate phase such as Cs_2AgBr_3 is involved, suggesting that the overall synthesis pathway remains energetically viable. Conversely, in instances where synthesis was unsuccessful, the pathways are characterized by positive $\Delta G_{\text{residual}}$, implying a tendency for intermediates to persist, possibly as residues, due to energetically unfavorable conditions.

A closer examination of cases that failed to synthesize reveals a link to the energy stability of the Cu octahedral site, as highlighted in previous research.³¹ The formation of the final phase $A_2B'(1+)B'(3+)X_6$ requires generation of the $B'(1+)X_6$ octahedral structure, in addition to the existing $B'(3+)X_6$ octahedral structure in the $A_3B'_2(3+)X_9$. However, for halides featuring Cu at the B-site, this transition is thermodynamically unfavorable and does not occur naturally. This results in a positive $\Delta G_{\text{residual}}$ particularly for double perovskite halides, where Cu occupies the B-site. Therefore, a more effective prediction of synthesizability can be achieved by employing Gibbs free energy of formation calculations that consider the entire reaction pathway, offering a robust method for predicting the material synthesizability of double perovskite halides. Furthermore, we validated our hypothesis by



Path	Predicted path	ΔG (eV/f.u)
1	$3\text{CsBr} + 2\text{BiBr}_3 \rightarrow \text{Cs}_3\text{Bi}_2\text{Br}_9$ $\text{Cs}_3\text{Bi}_2\text{Br}_9 + \text{CsBr} + 2\text{AgBr} \rightarrow 2\text{Cs}_2\text{AgBiBr}_6$	-1.16 -0.18
2	$3\text{CsBr} + 2\text{BiBr}_3 \rightarrow \text{Cs}_3\text{Bi}_2\text{Br}_9$ $2\text{CsBr} + \text{AgBr} \rightarrow \text{Cs}_2\text{AgBr}_3$ $2\text{Cs}_3\text{Bi}_2\text{Br}_9 + 3\text{AgBr} + \text{Cs}_2\text{AgBr}_3 \rightarrow 4\text{Cs}_2\text{AgBiBr}_6$	-1.16 -0.19 -0.13
3	$3\text{CsBr} + 2\text{BiBr}_3 \rightarrow \text{Cs}_3\text{Bi}_2\text{Br}_9$ $\text{CsBr} + \text{AgBr} \rightarrow \text{Cs}_2\text{AgBr}_3$ $\text{Cs}_3\text{Bi}_2\text{Br}_9 + \text{AgBr} + \text{Cs}_2\text{AgBr}_3 \rightarrow 2\text{Cs}_2\text{AgBiBr}_6$	-1.16 -0.12 -0.12



Path	Predicted path	ΔG (eV/f.u)
1	$3\text{CsBr} + 2\text{InBr}_3 \rightarrow \text{Cs}_3\text{In}_2\text{Br}_9$ $\text{Cs}_3\text{In}_2\text{Br}_9 + 3\text{Cs}_3\text{Cu}_2\text{Br}_5 + 4\text{CuBr} \rightarrow 8\text{Cs}_2\text{CuInBr}_6$	-1.15 0.26
2	$3\text{CsBr} + 2\text{InBr}_3 \rightarrow \text{Cs}_3\text{In}_2\text{Br}_9$ $3\text{CsBr} + 2\text{CuBr} \rightarrow \text{Cs}_3\text{Cu}_2\text{Br}_5$ $\text{Cs}_3\text{In}_2\text{Br}_9 + \text{Cs}_3\text{Cu}_2\text{Br}_5 + 4\text{CuBr} \rightarrow 8\text{Cs}_2\text{CuInBr}_6$	-1.15 -0.49 0.34
3	$3\text{CsBr} + 2\text{InBr}_3 \rightarrow \text{Cs}_3\text{In}_2\text{Br}_9$ $3\text{CsBr} + 2\text{CuBr} \rightarrow \text{Cs}_3\text{Cu}_2\text{Br}_5$ $\text{Cs}_3\text{In}_2\text{Br}_9 + \text{Cs}_3\text{Cu}_2\text{Br}_5 \rightarrow 2\text{Cs}_2\text{CuInBr}_6$	-1.15 -0.30 0.41

Figure 4. Reaction paths involving the $\text{A}_3\text{B}'_2\text{X}_9$ phase for (a) $\text{Cs}_2\text{AgBiBr}_6$ and (b) $\text{Cs}_2\text{CuInBr}_6$, sorted by the Gibbs free energy of formation in the negative direction. Predicted paths were derived using the CRN.

incorporating double perovskite halides, documented for solid-state synthesis in Table S1, and found a general alignment with the observed results.^{35,36} Following this, our findings demonstrated a level of accuracy comparable to that of the energy above the hull approach. However, it is worth noting that the energy above the hull approach revealed several synthesis instances with values above zero among perovskite halide candidates, a notable limitation (see the Supporting Information for details).

By integrating the reaction pathway analysis with the Gibbs free energy of formation calculations, we have achieved synthesizability predictions that align closely with experimental outcomes. We now turn to compare these findings with

established structural factors commonly used in assessing the stability of perovskite materials: the tolerance factor,⁹ the octahedral factor, and the new tolerance factor, which incorporates a machine learning descriptor.¹⁰ The traditional tolerance factor assesses the cubic resemblance of a perovskite structure, while the octahedral factor evaluates the potential for forming a stable BX_6 -type octahedral structure. The new tolerance factor, meanwhile, uses a machine learning descriptor to quantify the influence of the ion radii of A, B, and X ions on structural stability, with smaller values indicating a higher likelihood of perovskite formation.¹⁰

In Figure 7, we analyze these structural factors for the double perovskite halides listed in Table 1. The traditional tolerance factor suggests structural stability for all of the halides in Table 1, a prediction that contradicts experimental observations. The octahedral factor points to instability only in the case of $\text{Cs}_2\text{CuInBr}_6$. Interestingly, the presence of Cu at the B-site results in higher values of the new tolerance factor, indicating a lower stability. Yet, for compounds like $\text{Cs}_2\text{CuInCl}_6$, which have not been synthesized, all three structural factors indicate stability. This observation contrasts with our results, where we predicted that synthesizing $\text{Cs}_2\text{CuInCl}_6$ would be challenging. Such discrepancies highlight the subtle complexities in predicting the perovskite synthesizability and underscore the importance of incorporating a comprehensive reaction pathway analysis beyond traditional structural evaluations.

The discrepancy in predictions between our approach and traditional methods can be largely attributed to the consideration of the reaction pathways. Conventional approaches in perovskite research have predominantly focused on evaluating the structural stability. However, our analysis of compounds like $\text{Cs}_2\text{CuInCl}_6$ reveals additional layers of complexity. For instance, in the synthesis of $\text{Cs}_2\text{CuInCl}_6$, the initial formation of intermediate $\text{Cs}_3\text{In}_2\text{Cl}_9$ in the interfacial reaction demands a large driving force. This considerable initial energy requirement reduces the residual force for the subsequent conversion to $\text{Cs}_2\text{CuInCl}_6$. Moreover, this conversion process is energetically demanding, especially due to the characteristics of the Cu octahedral structure.³¹

By incorporating the reaction pathway into our analysis, we gain insights into factors such as the system's driving force and the intermediate octahedral structures. These factors play a crucial role in the synthesis process, often dictating the feasibility of the formation of the desired compound. Thus, by considering these additional elements, we can achieve a more accurate prediction of the synthesizability, surpassing what structural analysis alone can offer. This approach not only enhances our understanding of material synthesizability but also suggests new directions for optimizing synthesis strategies in perovskite research.

Our synthesizability predictions, derived from the reaction pathfinding approach, have been further applied to a wider array of double perovskite halides, as detailed in Table S2. Utilizing data sets from the Materials Project and ICSD,^{2,32} we meticulously selected candidates for which the $\text{A}_3\text{B}'_2\text{X}_9$ intermediate phase is theoretically plausible but has not been experimentally observed by solid-state synthesis. Among these, compounds like $\text{Cs}_2\text{AgYCl}_6$ and $\text{Cs}_2\text{KInCl}_6$,^{37,38} each potentially useful for γ -ray detection and as photoluminescent materials, respectively, are predicted to be synthesizable, as indicated by their negative $\Delta G_{\text{residual}}$. Intriguingly, these candidates also meet the criteria set by traditional measures

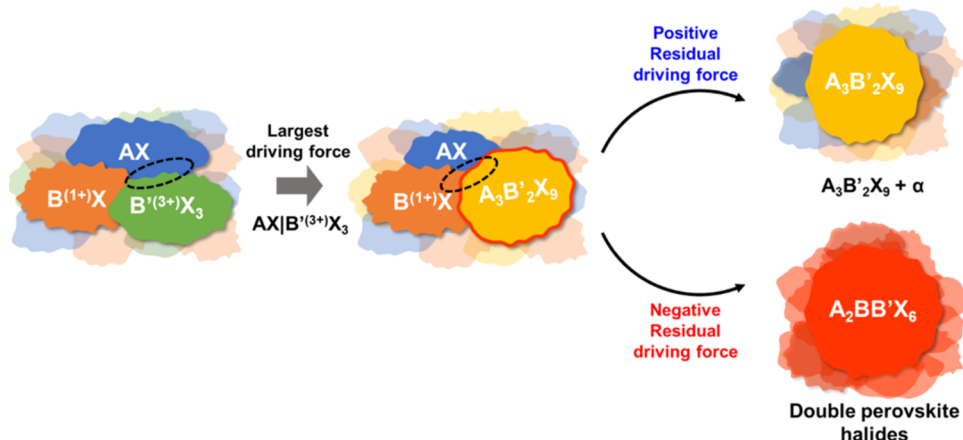


Figure 5. Schematic of the reaction path of the double perovskite halide based on the interface reaction and residual driving force.

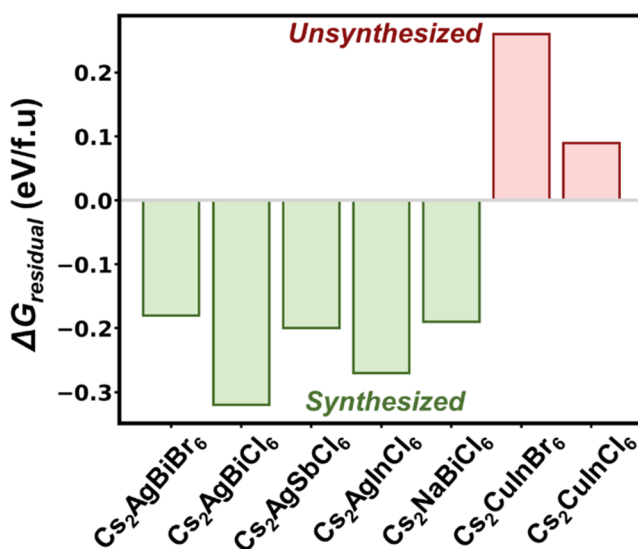


Figure 6. Residual Gibbs free energy of formation from the $A_3B'^{2}X_9$ intermediate to each double perovskite halide. The cases with the least energy among each reaction path were used.

of stability, including the conventional tolerance factor, octahedral factor, and new tolerance factor. Notably, all candidates predicted as synthesizable demonstrate a new tolerance factor of 4.016 or lower, underscoring their structural stability.

In instances in which synthesis was unsuccessful, several distinct trends emerged. First, candidates with Rb occupying the A site consistently exhibited a high positive overall $\Delta G_{\text{residual}}$, rendering them thermodynamically unfavorable for the identification of viable materials for synthesis. Second, candidates with an X site consisting of Iodine(I) displayed $\Delta G_{\text{residual}}$ values of at least 0.29 eV per formula unit. This contrasts with cases involving chlorine (Cl) and bromine (Br), where synthesizable candidates were identified. These observations provide valuable insights into the factors influencing synthesizability in double perovskite halides, indicating the effectiveness of our reaction pathfinding approach in complementing and enhancing traditional structural stability analyses. While currently focused on double perovskite halides, we look forward to expanding this methodology by exploring intermediates experimentally with

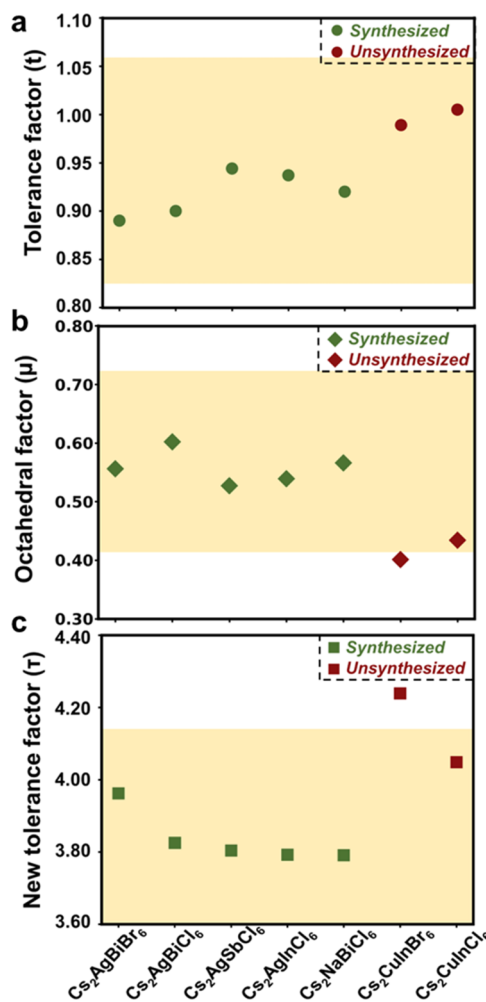


Figure 7. (a) Tolerance factor, (b) octahedral factor, and (c) new tolerance factor of double perovskite halides. The candidates were extracted from Table 1. The yellow area is a stable reference for each structural element.

in situ X-ray diffraction (XRD) and computationally through high-throughput methods.

4. CONCLUSIONS

In summary, our study presents a novel approach to predicting the synthesizability of double perovskite halides by focusing

closely on the reaction pathway. We have identified that the $A_3B'_2X_9$ phase, which indicates the strongest driving force, is likely to form as the initial intermediate through the interface reaction between AX and $B'^{(3+)}X_3$ precursors. Employing the CRN to analyze the reaction pathways that incorporate the $A_3B'_2X_9$ phase has revealed a key insight: high synthesizability is associated with scenarios where the residual Gibbs free energy of formation for the $A_2B^{(1+)}B'^{(3+)}X_6$ phase, derived from the $A_3B'_2X_9$ phase is negative. This approach potentially offers improvements over traditional structural factor analyses, especially in predicting the synthesizability of compounds that involve copper. Our methodology has not only suggested the synthesizability of known compounds but has also projected the potential for synthesizing several unexplored candidates. Notably, compounds such as Cs_2AgYCl_6 and Cs_2KinCl_6 have emerged as highly synthesizable in our study. These findings imply the importance of incorporating reaction pathways in synthesizability predictions, offering a more direct understanding of material synthesis. This enhanced approach points toward refining and advancing the field of materials science, particularly in the exploration and realization of novel double perovskite halides.

■ ASSOCIATED CONTENT

Data Availability Statement

The data that support the findings of this study are available from the corresponding author upon reasonable request.

■ Supporting Information

The Supporting Information is available free of charge at <https://pubs.acs.org/doi/10.1021/acs.chemmater.3c03323>.

Information on synthesizability prediction for double perovskite halides by structural factor and $\Delta G_{\text{residual}}$. Candidates are selected based on the identification of $A_3B'_2X_9$ phase in the Materials Project or ICSD. The generalized gradient approximation (GGA) within the Perdew–Burke–Ernzerhof (PBE) was used for the exchange–correlation potential ([PDF](#))

■ AUTHOR INFORMATION

Corresponding Author

Sung Beom Cho – Department of Energy Systems Research, Ajou University, Suwon 16499 Gyeonggi-do, Republic of Korea; Department of Material Science and Engineering, Ajou University, Suwon 16499 Gyeonggi-do, Republic of Korea; [orcid.org/0000-0002-3151-0113](#); Email: csb@ajou.ac.kr

Authors

Woongchan Kim – Department of Energy Systems Research, Ajou University, Suwon 16499 Gyeonggi-do, Republic of Korea; Department of Material Science and Engineering, Ajou University, Suwon 16499 Gyeonggi-do, Republic of Korea

Hyeon Woo Kim – Division of Materials Science and Engineering, Hanyang University, Seoul 04763, Republic of Korea; Nano Convergence Materials Center, Emerging Materials R&D Division, Korea Institute of Ceramic Engineering and Technology (KICET), Jinju 52851 Gyeongsangnam-do, Republic of Korea

Han Uk Lee – Department of Energy Systems Research, Ajou University, Suwon 16499 Gyeonggi-do, Republic of Korea;

Department of Material Science and Engineering, Ajou University, Suwon 16499 Gyeonggi-do, Republic of Korea

Min Sung Kang – Department of Energy Systems Research, Ajou University, Suwon 16499 Gyeonggi-do, Republic of Korea; Department of Material Science and Engineering, Ajou University, Suwon 16499 Gyeonggi-do, Republic of Korea

Dong Won Jeon – Department of Energy Systems Research, Ajou University, Suwon 16499 Gyeonggi-do, Republic of Korea; Department of Material Science and Engineering, Ajou University, Suwon 16499 Gyeonggi-do, Republic of Korea

Soo Won Heo – Nano Convergence Materials Center, Emerging Materials R&D Division, Korea Institute of Ceramic Engineering and Technology (KICET), Jinju 52851 Gyeongsangnam-do, Republic of Korea; [orcid.org/0000-0003-2064-1895](#)

Complete contact information is available at:
<https://pubs.acs.org/10.1021/acs.chemmater.3c03323>

Notes

The authors declare no competing financial interest.

■ ACKNOWLEDGMENTS

This research was supported by the Learning & Academic Research Institution for Master's Ph.D. Students and Postdocs (LAMP) Program of the National Research Foundation of Korea (NRF) grant funded by the Ministry of Education (RS-2023-00285390). The computational resources were provided by the Korea Supercomputing Center (KSC-2023-CRE-0387). This research was also supported by National R&D Program through the National Research Foundation of Korea (NRF) funded by the Ministry of Science and ICT (RS-2023-00209910, RS-2024-00407282).

■ REFERENCES

- (1) Schleder, G. R.; Padilha, A. C. M.; Acosta, C. M.; Costa, M.; Fazzio, A. From DFT to Machine Learning: Recent Approaches to Materials Science—a Review. *J. Phys.: Mater.* **2019**, *2* (3), No. 032001.
- (2) Jain, A.; Ong, S. P.; Hautier, G.; Chen, W.; Richards, W. D.; Dacek, S.; Cholia, S.; Gunter, D.; Skinner, D.; Ceder, G.; Persson, K. A. Commentary: The Materials Project: A Materials Genome Approach to Accelerating Materials Innovation. *APL Mater.* **2013**, *1* (1), No. 011002.
- (3) Kim, H. W.; Han, J. H.; Ko, H.; Samanta, T.; Lee, D. G.; Jeon, D. W.; Kim, W.; Chung, Y.-C.; Im, W. B.; Cho, S. B. High-Throughput Screening on Halide Perovskite Derivatives and Rational Design of Cs_3LuCl_6 . *ACS Energy Lett.* **2023**, *8* (8), 3621–3630.
- (4) Kahle, L.; Marcolongo, A.; Marzari, N. High-Throughput Computational Screening for Solid-State Li-Ion Conductors. *Energy Environ. Sci.* **2020**, *13* (3), 928–948.
- (5) Woods-Robinson, R.; Broberg, D.; Faghaninia, A.; Jain, A.; Dwaraknath, S. S.; Persson, K. A. Assessing High-Throughput Descriptors for Prediction of Transparent Conductors. *Chem. Mater.* **2018**, *30* (22), 8375–8389.
- (6) Emery, A. A.; Saal, J. E.; Kirklin, S.; Hegde, V. I.; Wolverton, C. High-Throughput Computational Screening of Perovskites for Thermochemical Water Splitting Applications. *Chem. Mater.* **2016**, *28* (16), 5621–5634.
- (7) Sun, W.; Dacek, S. T.; Ong, S. P.; Hautier, G.; Jain, A.; Richards, W. D.; Gamst, A. C.; Persson, K. A.; Ceder, G. The Thermodynamic Scale of Inorganic Crystalline Metastability. *Sci. Adv.* **2016**, *2* (11), No. e1600225.
- (8) Cai, Y.; Xie, W.; Teng, Y. T.; Harikesh, P. C.; Ghosh, B.; Huck, P.; Persson, K. A.; Mathews, N.; Mhaisalkar, S. G.; Sherburne, M.,

- Asta, M. High-Throughput Computational Study of Halide Double Perovskite Inorganic Compounds. *Chem. Mater.* **2019**, *31* (15), 5392–5401.
- (9) Goldschmidt, V. M. Die Gesetze Der Krystallochemie. *Naturwissenschaften* **1926**, *14* (21), 477–485.
- (10) Bartel, C. J.; Sutton, C.; Goldsmith, B. R.; Ouyang, R.; Musgrave, C. B.; Ghiringhelli, L. M.; Scheffler, M. New Tolerance Factor to Predict the Stability of Perovskite Oxides and Halides. *Sci. Adv.* **2019**, *5* (2), No. eaav0693.
- (11) Bai, J.; Sun, W.; Zhao, J.; Wang, D.; Xiao, P.; Ko, J. Y. P.; Huq, A.; Ceder, G.; Wang, F. Kinetic Pathways Tempered by Low-Temperature Intermediates during Solid-State Synthesis of Layered Oxides. *Chem. Mater.* **2020**, *32* (23), 9906–9913.
- (12) Chung, S.-Y.; Kim, Y.-M.; Kim, J.-G.; Kim, Y.-J. Multiphase Transformation and Ostwald's Rule of Stages during Crystallization of a Metal Phosphate. *Nat. Phys.* **2009**, *5* (1), 68–73.
- (13) Bianchini, M.; Wang, J.; Clément, R. J.; Ouyang, B.; Xiao, P.; Kitchaev, D.; Shi, T.; Zhang, Y.; Wang, Y.; Kim, H.; Zhang, M.; Bai, J.; Wang, F.; Sun, W.; Ceder, G. The Interplay between Thermodynamics and Kinetics in the Solid-State Synthesis of Layered Oxides. *Nat. Mater.* **2020**, *19* (10), 1088–1095.
- (14) Miura, A.; Bartel, C. J.; Goto, Y.; Mizuguchi, Y.; Moriyoshi, C.; Kuroiwa, Y.; Wang, Y.; Yaguchi, T.; Shirai, M.; Nagao, M.; Rosero-Navarro, N. C.; Tadanaga, K.; Ceder, G.; Sun, W. Observing and Modeling the Sequential Pairwise Reactions That Drive Solid-State Ceramic Synthesis. *Adv. Mater.* **2021**, *33* (24), No. e2100312.
- (15) Sun, Q.; Yin, W.-J.; Wei, S.-H. Searching for Stable Perovskite Solar Cell Materials Using Materials Genome Techniques and High-Throughput Calculations. *J. Mater. Chem. C* **2020**, *8* (35), 12012–12035.
- (16) Islam, M. S.; Wang, S.; Nolan, A. M.; Mo, Y. First-Principles Computational Design and Discovery of Novel Double-Perovskite Proton Conductors. *Chem. Mater.* **2021**, *33* (21), 8278–8288.
- (17) Li, Z.; Xu, Q.; Sun, Q.; Hou, Z.; Yin, W. Thermodynamic Stability Landscape of Halide Double Perovskites via High-Throughput Computing and Machine Learning. *Adv. Funct. Mater.* **2019**, *29* (9), No. 1807280.
- (18) Talapatra, A.; Uberuaga, B. P.; Stanek, C. R.; Pilania, G. A Machine Learning Approach for the Prediction of Formability and Thermodynamic Stability of Single and Double Perovskite Oxides. *Chem. Mater.* **2021**, *33* (3), 845–858.
- (19) Liang, G.-Q.; Zhang, J. A Machine Learning Model for Screening Thermodynamic Stable Lead-Free Halide Double Perovskites. *Comput. Mater. Sci.* **2022**, *204*, No. 111172.
- (20) Kresse, G.; Furthmüller, J. Efficient Iterative Schemes for Ab Initio Total-Energy Calculations Using a Plane-Wave Basis Set. *Phys. Rev. B* **1996**, *54* (16), 11169–11186.
- (21) Blöchl, P. E. Projector Augmented-Wave Method. *Phys. Rev. B* **1994**, *50* (24), 17953–17979.
- (22) Perdew, J. P.; Burke, K.; Ernzerhof, M. Generalized Gradient Approximation Made Simple. *Phys. Rev. Lett.* **1996**, *77* (18), 3865–3868.
- (23) Furness, J. W.; Kaplan, A. D.; Ning, J.; Perdew, J. P.; Sun, J. Accurate and Numerically Efficient R2SCAN Meta-Generalized Gradient Approximation. *J. Phys. Chem. Lett.* **2020**, *11* (19), 8208–8215.
- (24) Ouyang, R.; Curtarolo, S.; Ahmetcik, E.; Scheffler, M.; Ghiringhelli, L. M. SISSO: A Compressed-Sensing Method for Identifying the Best Low-Dimensional Descriptor in an Immensity of Offered Candidates. *Phys. Rev. Mater.* **2018**, *2* (8), No. 083802.
- (25) Bartel, C. J.; Millican, S. L.; Deml, A. M.; Rumptz, J. R.; Tumas, W.; Weimer, A. W.; Lany, S.; Stevanović, V.; Musgrave, C. B.; Holder, A. M. Physical Descriptor for the Gibbs Energy of Inorganic Crystalline Solids and Temperature-Dependent Materials Chemistry. *Nat. Commun.* **2018**, *9* (1), No. 4168.
- (26) McDermott, M. J.; Dwaraknath, S. S.; Persson, K. A. A Graph-Based Network for Predicting Chemical Reaction Pathways in Solid-State Materials Synthesis. *Nat. Commun.* **2021**, *12* (1), No. 3097.
- (27) McClure, E. T.; Ball, M. R.; Windl, W.; Woodward, P. M. Cs₂AgBiX₆ (X = Br, Cl): New Visible Light Absorbing, Lead-Free Halide Perovskite Semiconductors. *Chem. Mater.* **2016**, *28* (5), 1348–1354.
- (28) Udadant, R.; Thawarkar, S.; Rondiya, S.; Shelke, A.; Aher, R.; Ajithkumar, T. G.; Cross, R. W.; Dzade, N. Y.; Jadkar, S. Lead-Free Solid State Mechanochemical Synthesis of Cs₂NaBi_{1-x}Fe_xCl₆ Double Perovskite: Reduces Band Gap and Enhances Optical Properties. *Inorg. Chem.* **2023**, *62* (12), 4861–4871.
- (29) Tran, T. T.; Panella, J. R.; Chamorro, J. R.; Morey, J. R.; McQueen, T. M. Designing Indirect–Direct Bandgap Transitions in Double Perovskites. *Mater. Horiz.* **2017**, *4* (4), 688–693.
- (30) Zhao, F.; Song, Z.; Zhao, J.; Liu, Q. Double Perovskite Cs₂AgInCl₆: Broadband and near-Infrared Luminescent Materials. *Inorg. Chem. Front.* **2019**, *6* (12), 3621–3628.
- (31) Xiao, Z.; Du, K.; Meng, W.; Mitzi, D. B.; Yan, Y. Chemical Origin of the Stability Difference between Copper(I)- and Silver(I)-Based Halide Double Perovskites. *Angew. Chem.* **2017**, *129* (40), 12275–12279.
- (32) Hellenbrandt, M. The Inorganic Crystal Structure Database (ICSD)—Present and Future. *Crystallogr. Rev.* **2004**, *10* (1), 17–22.
- (33) Tang, Y.; Liang, M.; Chang, B.; Sun, H.; Zheng, K.; Pullerits, T.; Chi, Q. Lead-Free Double Halide Perovskite Cs₃BiBr₆ with Well-Defined Crystal Structure and High Thermal Stability for Optoelectronics. *J. Mater. Chem. C* **2019**, *7* (11), 3369–3374.
- (34) Meyer, G. Zur Kenntnis Der Chloro- Und Bromo-Indate (III). A₃In₂Cl₉ (A = Cs, Rb, In, Tl) Und Cs₃In₂Br_{9-x}Cl_x (x = 0, 3, 6, 7, 8). *Z. Anorg. Allg. Chem.* **1978**, *445* (1), 140–146.
- (35) Xiao, Z.; Du, K.-Z.; Meng, W.; Wang, J.; Mitzi, D. B.; Yan, Y. Intrinsic Instability of Cs₂In(1)M(III)X₆ (M = Bi, Sb; X = Halogen) Double Perovskites: A Combined Density Functional Theory and Experimental Study. *J. Am. Chem. Soc.* **2017**, *139* (17), 6054–6057.
- (36) Zhou, Y.; Askar, A. M.; Pöhls, J.; Iyer, A. K.; Oliynyk, A. O.; Shankar, K.; Mar, A. Hexagonal Double Perovskite Cs₂AgCrCl₆. *Z. Anorg. Allg. Chem.* **2019**, *645* (3), 323–328.
- (37) Du, M.-H.; Biswas, K. Electronic Structure Engineering of Elpasolites: Case of Cs₂AgYCl₆. *J. Lumin.* **2013**, *143*, 710–714.
- (38) Huang, W.; Peng, H.; Wei, Q.; Xia, J.; He, X.; Ke, B.; Tian, Y.; Zou, B. Tunable Efficient White Emission in Holmium Doped Double Perovskites Cs₂KInCl₆ via Antimony Sensitization. *Adv. Opt. Mater.* **2023**, *11* (10), No. 2203103, DOI: [10.1002/adom.202203103](https://doi.org/10.1002/adom.202203103).